2012-2-15

Self-Calibration for Three-Point Intrinsic Alignment Autocorrelations in Weak Lensing Surveys

Michael A. Troxel and Mustapha Ishak-Boushaki

This article has been accepted for publication in the Monthly Notices of the Royal Astronomical Society

Monthly Notices
of the
ROYAL ASTRONOMICAL SOCIETY

Mon. Not. R. Astron. Soc. **423,** 1663–1673 (2012) doi:10.1111/j.1365-2966.2012.20987.x

Self-calibration for three-point intrinsic alignment autocorrelations in weak lensing surveys

M. A. Troxel★ and M. Ishak★

Department of Physics, The University of Texas at Dallas, Richardson, TX 75083, USA

Accepted 2012 March 23. Received 2012 March 23; in original form 2012 February 15

ABSTRACT

The weak lensing signal (cosmic shear) has been shown to be strongly contaminated by the various types of galaxy intrinsic alignment (IA) correlations, which poses a barrier to precision weak lensing measurements. The redshift dependence of the IA signal has been used at the two-point level to reduce this contamination by only measuring cross-correlations between large redshift bins, which significantly reduces the galaxy intrinsic ellipticity–intrinsic ellipticity (II) correlation. A self-calibration technique based on the redshift dependencies of the IA correlations has also been proposed as a means to remove the two-point IA contamination from the lensing signal. We explore here the redshift dependencies of the IA and lensing bispectra in order to propose a self-calibration of the IA autocorrelations at the three-point level (i.e. GGI, GII and III), which can be well understood without the assumption of any particular IA model. We find that future weak lensing surveys will be able to measure the distinctive IA redshift dependence over ranges of $|\Delta z^{\rm P}| \leq 0.2$. Using conservative estimates of photo-z accuracy, we describe the three-point self-calibration technique for the total IA signal, which can be accomplished through lensing tomography of photo-z bin size $\sim$0.01. We find that the three-point self-calibration can function at the accuracy of the two-point technique with modest constraints in redshift separation. This allows the three-point IA autocorrelation self-calibration technique proposed here to significantly reduce the contamination of the IA contamination to the weak lensing bispectrum.

Key words: gravitational lensing: weak – cosmological parameters.

1 INTRODUCTION

Originally just a prediction of general relativity, gravitational lensing has recently emerged as an independent means to make precision astrophysical and cosmological measurements, which are blind to the exact nature of the lens mass. This is particularly true for weak lensing due to large-scale structure (cosmic shear), which is able to map structure composed of both visible matter as well as dark matter, which is primarily detectable through its gravitational signal only. The importance of this new probe has spurred the development of a new generation of ground- and space-based surveys suited for precision weak lensing measurements. These ongoing, future and proposed surveys [e.g. CFHTLS (http://www.cfht.hawaii..edu/Science/CFHLS/), DES (http://www.darkenergysurvey.org/), *Euclid* (http://sci.esa.int/euclid/), HSC (http://www.naoj.org/Projects/HSC/), *Hubble Space Telescope* (*HST*; http://www.stsci.edu/hst/), *James Webb Space Telescope* (http://www.jwst.nasa.gov/), LSST (http://www.lsst.org/lsst/), Pan-STARRS (http://pan-starrs.ifa.hawaii.edu/) and WFIRST (http://wfirst.gsfc.nasa.gov/)] promise to provide greatly improved measurements of cosmic shear using the shapes of up to billions of galaxies. These cosmic measurements allow us to not only characterize the equation of state of dark energy, but when combined with other probes can improve constraints on the equation of state of dark energy and the matter fluctuation amplitude parameter by factors of 2–4 (see e.g. Zaldarriaga, Spergel & Seljak 1997; Eisenstein, Hu & Tegmark 1999; Hu & Tegmark 1999; Bacon, Refregier & Ellis 2000; Van Waerbeke et al. 2000, 2002; Rhodes, Refregier & Groth 2001; Hoekstra et al. 2002; Hu 2002; Brown et al. 2003; Jarvis et al. 2003; Pen et al. 2003; Ishak 2005, 2007; Massey et al. 2005; Upadhye, Ishak & Steinhardt 2005; Fu, Wu & Yu 2009; Joudaki, Cooray & Holz 2009; Schrabback et al. 2010, and references therein). Weak lensing has also been shown to be very useful to test the nature of gravity at cosmological distance scales (see e.g. the partial list Song 2005; Capozziello, Cardone & Troisi 2006; Ishak, Upadhye & Spergel 2006; Zhao et al. 2006, 2009; Huterer & Linder 2007; Linder & Cahn 2007; Zhang et al. 2007; Acquaviva et al. 2008; Daniel et al. 2008, 2010; Schmidt 2008; Ishak & Dossett 2009; Thomas, Abdalla & Weller 2009;

★E-mail: troxel@utdallas.edu (MAT); mishak@utdallas.edu (MI)

Bean & Tangmatitham 2010; Tereno, Semboloni & Schrabback 2010; Dossett, Moldenhauer & Ishak 2011).

The three-point cosmic shear correlation and the shear bispectrum have been shown to break degeneracies in the cosmological parameters in addition to the constraints obtained from the two-point cosmic shear correlation and the corresponding shear power spectrum that the power spectrum alone does not break (Takada & Jain 2003; Vafaei et al. 2010). For example, the results of Takada & Jain (2004) showed that a deep lensing survey should be able to improve the constraints on the dark energy parameters and the matter fluctuation amplitude by a further factor of 2–3 using the bispectrum. Most recently, Semboloni et al. (2010) derived parameter constraints by measuring the third-order moment of the aperture mass measure using weak lensing data from the *HST* COSMOS survey. They found independent results consistent with 7-year *Wilkinson Microwave Anisotropy Probe* best-fitting cosmology and an improved constraint when combined with the two-point correlation. In addition to improved parameter constraints, by definition the bispectrum also allows us to explore information about non-Gaussianity in the universe that is inaccessible at the two-point level, providing constraints on the degree of non-Gaussianity (see e.g. Matarrese, Verde & Jimenez 2000; Verde et al. 2001; Takada & Jain 2004; Jeong & Komatsu 2009; Huterer, Komatsu & Shandera 2010; Munshi et al. 2012, and references therein).

As we describe below, we extend in this paper the two-point self-calibration technique proposed by Zhang (2010b) to the three-point intrinsic alignment autocorrelation bispectra between galaxies in a single redshift bin. This technique is different from the cross-correlation techniques proposed in Zhang (2010a) and Troxel & Ishak (2012a), instead using differences in the redshift dependencies of the intrinsic alignment and lensing bispectra to self-calibrate the intrinsic alignment signal. These two- and three-point intrinsic alignment correlations constitute a contaminant to the lensing signal and must be isolated and removed to avoid biasing the cosmological information contained within the cosmic shear power spectra and bispectra.

Cosmic shear measurements are in fact limited in precision by several systematic effects which must be accounted for in order to make full use of the potential of future weak lensing surveys (see e.g. Croft & Metzler 2000; Heavens, Refregier & Heymans 2000; Bacon et al. 2001; Catelan, Kamionkowski & Blandford 2001; Erben et al. 2001; Bernstein & Jarvis 2002; Brown et al. 2002; King & Schneider 2002; Hirata & Seljak 2003a; Refregier 2003; Van Waerbeke & Mellier 2003; Heymans et al. 2004; Ishak et al. 2004; Takada & White 2004, and references therein), and one of the serious systematic effects of weak lensing is this correlated intrinsic alignment of galaxy ellipticities, which acts as a nuisance factor (see e.g. Croft & Metzler 2000; Catelan et al. 2001; Crittenden et al. 2001; Brown et al. 2002; Jing 2002; King & Schneider 2002, 2003; Heymans & Heavens 2003; Hirata & Seljak 2003b, 2004; King 2005; Heymans et al. 2006; Mandelbaum et al. 2006; Bridle & King 2007; Hirata et al. 2007; Semboloni et al. 2008; Faltenbacher et al. 2009; Okumura & Jing 2009; Joachimi & Bridle 2010; Joachimi et al. 2010; Kirk, Bridle & Schneider 2010; Blazek, McQuinn & Seljak 2011; Krause & Hirata 2011; Troxel & Ishak 2012b, and references therein). For example, Bridle & King (2007) and Joachimi & Bridle (2010) showed that if intrinsic alignment is ignored, the determination of the dark energy equation of state is biased by as much as 50 per cent. Hirata et al. (2007) found that the matter power spectrum amplitude can be affected by intrinsic alignment by up to 30 per cent, showing the importance of developing methods to isolate the intrinsic alignment and remove it from the cosmic shear signal.

There are two two-point intrinsic alignment correlations. The first is a correlation between the intrinsic ellipticity of two galaxies, known as the II correlation. If the two galaxies are spatially close, they can be aligned by the tidal force field of the same nearby matter structure. The second intrinsic alignment correlation, known as the GI correlation, was identified by Hirata & Seljak (2004) and is due to a matter structure both causing the alignment of a nearby galaxy and contributing to the lensing signal of a background galaxy. This produces an anticorrelation between the cosmic shear and intrinsic ellipticity, since the tidal force and gravitational lensing tend to align the galaxy shapes in orthogonal directions. We represent these correlations diagrammatically in Fig. 1. The GI correlation has been measured in various subsets of the Sloan Digital Sky Survey (SDSS) spectroscopic and imaging samples by various groups. A detection of the large-scale GI correlation in the SDSS was reported by Mandelbaum et al. (2006), and then Hirata et al. (2007) found an even stronger GI correlation for luminous red galaxies (LRGs). It was shown in these papers that this contamination can affect the lensing measurement and cosmology up to the 10 per cent level and up to 30 per cent in some cases for the matter fluctuation amplitude. This finding was confirmed by numerical simulations, where a level of contamination of 10 per cent was found (Heymans et al. 2006). Further measurements of the GI correlation were made in the SDSS data set by Faltenbacher et al. (2009) and Okumura & Jing (2009). Most recently, Joachimi et al. (2010) measured strong two-point intrinsic alignment correlations in various SDSS and MegaZ–LRG samples.

In a similar way, when we consider three galaxies and the related three-point correlation, the cosmic shear signal (GGG bispectrum) also suffers from contamination by the three-point intrinsic alignment correlations. The first is the III correlation between intrinsic ellipticities of three spatially close galaxies which are intrinsically aligned by a nearby matter structure. The second is the GII correlation, where two spatially close galaxies are intrinsically aligned by a nearby matter structure which contributes to the lensing of a third galaxy in the background. Finally, there is the GGI correlation, where two galaxies are lensed by a structure which intrinsically aligns a third galaxy in the foreground. Unlike the two-point correlations, the sign of the GGI and GII correlations depends both on triangle shape and scale. The three-point intrinsic alignment correlations are represented diagrammatically in Fig. 2. Semboloni et al. (2008) showed that lensing bispectrum measurements are typically more strongly contaminated by intrinsic alignment compared to the lensing spectrum measurements, and that the contamination from the three-point intrinsic alignment correlation can be as large as 15–20 per cent compared to the GGG lensing signal. The three-point intrinsic alignment measurements are not only useful for constraining their contamination to three-point lensing measurements, but are also useful for constraining models of intrinsic alignments and therefore constraining the contamination to all lensing measurements (including two-point correlations) which will dominate the science cases of upcoming surveys.

While the II, III and GII intrinsic alignment correlations can be greatly reduced with photo-z by using cross-spectra of galaxies in two different redshift bins (see e.g. Refregier 2003) so that the galaxies are separated by large enough distances to assure that the tidal effect is weak, this does not work for the GI and GGI correlations which remain strong between galaxies at different redshifts and large separations. The GI correlation and

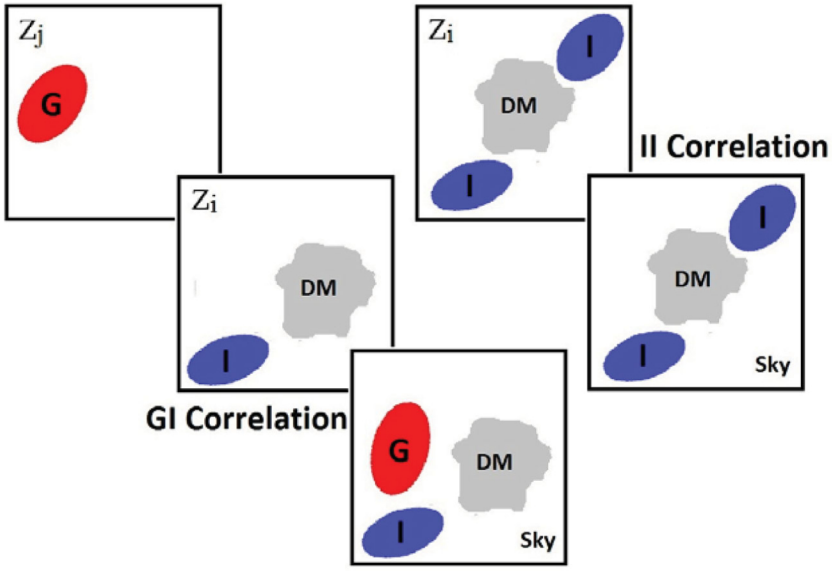

Figure 1. The two-point intrinsic alignment correlations. Galaxies which are intrinsically aligned are coloured in blue and labelled I, while galaxies which are lensed are coloured in red and labelled G. The lower right panels represent the view of the system on the sky, while each panel preceding it is at some distinct redshift where $z_i < z_j$. If the two galaxies are spatially close, at nearly the same redshift and angular position on the sky, they can be aligned by the tidal force field of the same nearby matter structure (labelled DM in the figure). This is shown as the II correlation. If instead a matter structure causes both the alignment of a nearby galaxy and contributes to the lensing signal of a background galaxy, this produces an anticorrelation with negative sign between the cosmic shear and intrinsic ellipticity, since the tidal force and gravitational lensing tend to align the galaxy shapes in orthogonal directions, and is shown as the GI correlation.

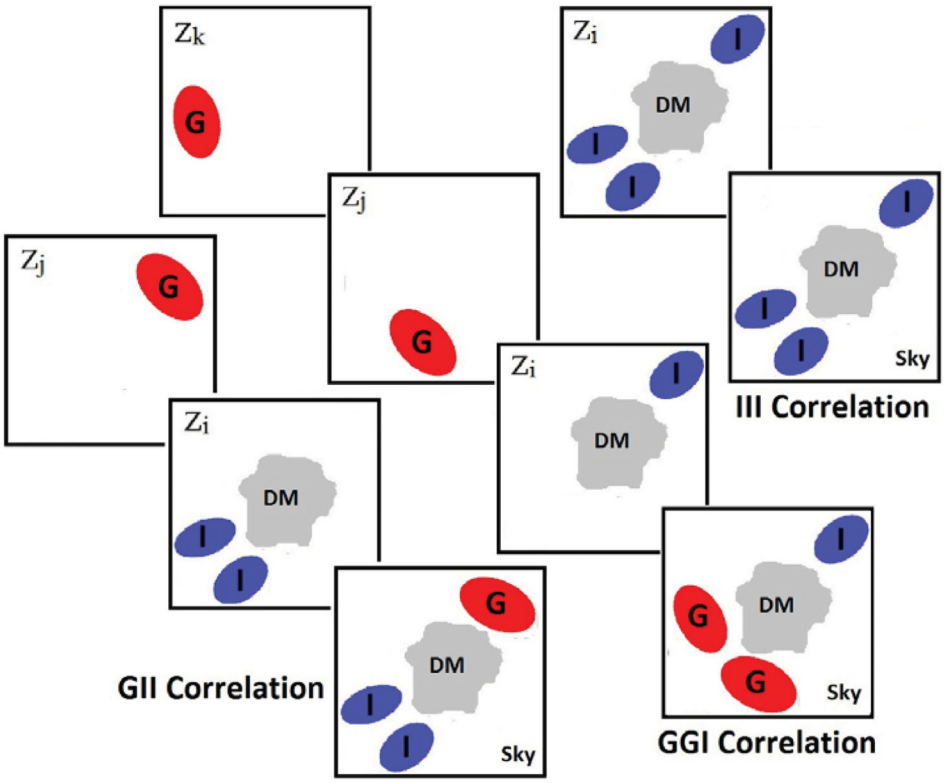

Figure 2. The three-point intrinsic alignment correlations. Galaxies which are intrinsically aligned are coloured in blue and labelled I, while galaxies which are lensed are coloured in red and labelled G. The lower right panels represent the view of the system on the sky, while each panel preceding it is at some distinct redshift where $z_i < z_j < z_k$. The III correlation is between the intrinsic ellipticities of three spatially close galaxies which are intrinsically aligned by a nearby matter structure (labelled DM in the figure). If instead two spatially close galaxies are intrinsically aligned by a nearby matter structure which contributes to the lensing of a third galaxy in the background, we label this the GII correlation. Finally, the GGI correlation is where two galaxies are lensed by a structure which intrinsically aligns a third galaxy in the foreground. Unlike the two-point correlations, the sign of the GGI and GII correlations can depend both on triangle shape and scale.

methods for its removal have been the topic of several recent scientific publications and we review these briefly. Initially, some first suggestions were discussed by Hirata & Seljak (2004). King (2005) extended the approach of template fitting by King & Schneider (2003) to include a treatment of the GI correlation. Bridle & King (2007) and Joachimi & Bridle (2010) investigated the effects of the GI correlation on cosmological parameter constraints by assuming a model of the GI intrinsic alignment that is binned in redshift and angular frequency with some free parameters that are marginalized over. Kirk et al. (2010) performed a cosmological constraint analysis where modelling of intrinsic alignment was included, showing a significant effect on the amplitude of matter fluctuations. Using a geometrical approach, Joachimi & Schneider (2008, 2009, 2010) proposed a nulling technique to remove the GI intrinsic alignment contribution by exploiting the redshift dependence of the correlations, but it was found that the technique throws out some of the valuable lensing signal. Most recently, the nulling technique has been applied at the three-point level for the GGI correlation, but again with similar signal loss to that at the two-point level (Shi, Joachimi & Schneider 2010). Finally, Zhang (2010a) proposed a technique to self-calibrate the GI intrinsic alignment signal by using additional galaxy density (cross-)correlations which are already present in weak lensing survey measurements. This approach was successfully extended in recent work by Troxel & Ishak (2012a) to the GGI cross-correlation bispectrum. Joachimi & Bridle (2010) applied an approach like the self-calibration, using correlations between lensing, intrinsic alignment, number density and magnification effects to constrain cosmological parameters. They found that the extra information from the additional correlations can make up for the additional free parameters in the intrinsic alignment so that the contamination can be removed without loss of constraining power.

Most recently, Zhang (2010b) showed that redshift dependencies of the intrinsic alignment spectra can allow further improvements to the calculation of the intrinsic alignment contamination. Zhang (2010b) demonstrates the strong redshift separation dependence of the two-point GI and II intrinsic alignment signals by considering the lensing and intrinsic alignment spectra due to galaxies in a single redshift bin that are at fixed photo-z separations $\Delta z^{\rm P}$ relative to some mean redshift. This results in a relative change in magnitude of the GI and II spectra of 50–60 per cent, but only a few per cent for GG at separation $\Delta z^{\rm P} = 0.2$. This corresponds to a decrease in 10 per cent of the total ellipticity power spectrum, which is identifiable in proposed surveys. Parametrizing the intrinsic alignment spectra as proportional to various galaxy density (cross-)spectra, this allows us to calculate and remove the intrinsic alignment component of the lensing signal. In this work we propose a method to extend this self-calibration technique to the three-point statistics, using instead the redshift dependencies of the GGI, GII and III bispectra, in order to calculate and remove the intrinsic alignment contamination to the lensing bispectrum.

We organize the paper as follows. In Section 2, we briefly discuss the necessary survey parameters and lensing formalism for the bispectrum. In Section 2.1, we discuss several methods to vary the redshift separation of galaxies in the bispectrum and compare the resulting redshift dependencies. Section 2.2 describes the analytical motivation and framework for the self-calibration using the redshift dependencies of the GGG, GGI, GII and III bispectra. We explore the performance of the self-calibration in Section 3.1, and discuss possible additional sources of error in the analysis in Section 3.2. Finally, we summarize the self-calibration and its applicability to future weak lensing surveys in Section 3 and discuss its impact in Section 4.

2 REDSHIFT SEPARATION DEPENDENCE IN THE BISPECTRUM

The galaxy intrinsic alignment and cosmic shear bispectra have very distinct dependencies on the redshift separation and orientation of the three galaxies, which we will explore and quantify in order to identify and measure the contribution of the intrinsic alignment to the measured ellipticity bispectrum. We work with the bispectrum $B^{\alpha\beta\gamma}(\ell; z_1^{\rm P}, z_2^{\rm P}, z_3^{\rm P})$, where α, β, $\gamma \in G, I, g$, which measures α at photometric redshift $z_1^{\rm P}$, β at $z_2^{\rm P}$ and γ at $z_3^{\rm P}$. We have denoted the lensing convergence as G, the galaxy intrinsic ellipticity as I and the galaxy density as g. Since we are only interested in exploring the redshift separation and orientation dependence of the bispectra, we will work at a fixed multipole ℓ and mean redshift $\bar{z}^{\rm P} = (z_1^{\rm P} + z_2^{\rm P} + z_3^{\rm P})/3$. In order to best compare to work on the power spectrum by Zhang (2010b), we will use equilateral triangles with $\ell = 1000$ and $\bar{z}^{\rm P} = 1.0$, unless otherwise stated, for which values the bispectrum will be measured to high confidence in planned weak lensing surveys. Unlike for the power spectrum, there are several possible choices in exploring the dependence on redshift separation, which we will discuss and compare in Section 2.1.

In our calculations we assume a standard, flat Λ cold dark matter universe. In the Born approximation, the convergence κ of a source galaxy at comoving distance $\chi_{\rm G}$ and direction $\hat{\theta}$ is then related to the matter density δ through the lensing kernel $W_{\rm L}(z', z)$ by

$$\kappa(\hat{\theta}) = \int_0^{\chi_{\rm G}} \delta(\chi_{\rm L}, \hat{\theta}) W_{\rm L}(\chi_{\rm L}, \chi_{\rm G})\, {\rm d}\chi_{\rm L}. \tag{1}$$

The three-dimensional (3D) matter bispectrum is then defined from the convergence as

$$\langle \tilde{\kappa}(\boldsymbol{\ell}_1)\tilde{\kappa}(\boldsymbol{\ell}_2)\tilde{\kappa}(\boldsymbol{\ell}_3)\rangle = (2\pi)^2 \delta^{\rm D}(\boldsymbol{\ell}_1 + \boldsymbol{\ell}_2 + \boldsymbol{\ell}_3) B(\ell_1, \ell_2, \ell_3), \tag{2}$$

where $\langle\cdots\rangle$ denotes the ensemble average and $\delta^{\rm D}(\boldsymbol{\ell})$ is the Dirac delta function. For the bispectrum, $\delta^{\rm D}(\boldsymbol{\ell}_1 + \boldsymbol{\ell}_2 + \boldsymbol{\ell}_3)$ enforces the condition that the three vectors form a triangle in Fourier space. Under the Limber approximation, we can express the 2D angular autocorrelation bispectrum as

$$B^{\alpha\beta\gamma}\left(\ell; z_1^{\rm P}, z_2^{\rm P}, z_3^{\rm P}\right) = \int_0^{\chi} \frac{W^{\alpha\beta\gamma}(\chi'; \chi_1, \chi_2, \chi_3)}{\chi'^4} B_{\alpha\beta\gamma}(k; \chi')\, {\rm d}\chi', \tag{3}$$

where for example when $\alpha = \beta = \gamma = G$, $B_{\rm GGG}(k; \chi')$ is the 3D matter bispectrum shown in equation (2). However, generally α, β, $\gamma \in G, I, g$, where the additional intrinsic alignment (I) and galaxy (g) bispectra are calculated as described further in Section 2.1. The redshift is simply related to χ through the Hubble parameter, $H(z)$. We can then write the weighting function in terms of redshift as

$$W^{\alpha\beta\gamma}\left(z(\chi); z_1^{\rm P}(\chi_1), z_2^{\rm P}(\chi_2), z_3^{\rm P}(\chi_3)\right) \equiv W^{\alpha}\left(z, z_1^{\rm P}\right) W^{\beta}\left(z, z_2^{\rm P}\right) \times W^{\gamma}\left(z, z_3^{\rm P}\right), \tag{4}$$

$$W^{\rm G}(z, z^{\rm P}) = \int_0^{\infty} W_{\rm L}(z', z) p(z'|z^{\rm P})\, {\rm d}z', \tag{5}$$

$$W^{\rm I}(z, z^{\rm P}) = W^{\rm g}(z, z^{\rm P}) = p(z|z^{\rm P}), \tag{6}$$

where $p(z|z^{\rm P})$ is the photo-z probability distribution function (PDF). In order to quantitatively examine the redshift separation dependence of the bispectra, we assume a specific form of the PDF

modelled after Ma & Bernstein (2008) with which to describe the photo-z uncertainty in a future weak lensing survey:

$$p(z|z^{\rm P}) = \frac{1-p_{\rm cat}}{\sqrt{2\pi}\sigma(z^{\rm P})}\exp\left[\frac{(z-z^{\rm P})^2}{2\sigma^2(z^{\rm P})}\right] + \frac{p_{\rm cat}}{\sqrt{2\pi}\sigma(z^{\rm P})} \times \exp\left[\frac{(z-f_{\rm bias}z^{\rm P})^2}{2\sigma^2(z^{\rm P})}\right]. \quad (7)$$

The fraction of outlier galaxies is given by $p_{\rm cat}$, with a true redshift which is biased by a factor $f_{\rm bias}$. We adopt similar values to Zhang, with $\sigma(z^{\rm P}) = 0.05(1+z^{\rm P})$, $p_{\rm cat} = 0.02$ and $f_{\rm bias} = 0.5$. These parameters are chosen to represent the expected photo-z accuracy of a stage IV weak lensing survey at $z^{\rm P} \approx 1$. We maintain the very conservative fraction of catastrophic outliers used by Zhang, which is a factor of 20 greater than the required fraction in a stage IV dark energy survey, where $p_{\rm cat} < 0.1$ per cent (Bernstein & Huterer 2009; Hearin et al. 2010). Typically we assume that $B^{\rm GGI}(\ell; z_1, z_2, z_3)$ is zero for $z_1, z_2 < z_3$ and that $B^{\rm GII}(\ell; z_1, z_2, z_3)$ is zero for $z_1 < z_2, z_3$ or $z_2 \neq z_3$, due to lensing geometry and the redshift separation and orientation dependence of the intrinsic alignment signal discussed in detail in Section 2.1 (Troxel & Ishak 2012a). However, due to sometimes large photo-z error, this is not always the case, so when referencing the GGI and GII correlations, we will instead work with the sums $B^{\rm GGI} + B^{\rm GIG} + B^{\rm IGG}$ and $B^{\rm GII} + B^{\rm IGI} + B^{\rm IIG}$, respectively.

2.1 Evaluating the redshift separation dependence

We calculate the required lensing, intrinsic alignment and galaxy bispectra using the relations and methods developed in Troxel & Ishak (2012a,b). We assume a deterministic galaxy bias for the galaxy bispectra, while the intrinsic alignment signal is calculated using the model of Schneider & Bridle (2010, hereafter SB10), which is based on the halo model prescription. We have used the fiducial parameters of their fitting formulae as listed in their tables I and II, with C_1 estimated by comparison to fig. 2 of Hirata & Seljak (2004). By design, this model reduces to the linear alignment model of Hirata & Seljak (2004) at large scale, but aims for a more motivated model of intrinsic alignment at small scales. For comparison, we also use the toy model adopted by Zhang (2010b), where the intrinsic alignment spectrum has a simple bias $b^{\rm I}(k,z) \propto [1+\Delta^2_{\rm m}(k,z)]^a$ ($a \in [0, 1/2]$), where $\Delta^2_{\rm m}(k,z)$ is the 3D matter power spectrum. This allows us to evaluate the behaviour of the redshift separation and orientation dependence of the bispectrum for a wide range of intrinsic alignment dependence on both scale and redshift.

We relate the flat-sky bispectrum to the all-sky bispectrum through the Wigner-3j symbol, where

$$B^{\alpha\beta\gamma}_{ijk,\ell_1\ell_2\ell_3} \approx \begin{pmatrix} \ell_1 & \ell_2 & \ell_3 \\ 0 & 0 & 0 \end{pmatrix} \sqrt{\frac{(2\ell_1+1)(2\ell_2+1)(2\ell_3+1)}{4\pi}} B^{\alpha\beta\gamma}_{ijk}(\ell_1,\ell_2,\ell_3). \quad (8)$$

We calculate the Wigner-3j symbol following the approximation given in appendix A of Takada & Jain (2004). We then compute the 3D bispectrum due to non-linear gravitational clustering, $B_\delta(k_1, k_2, k_3; \chi)$, following the fitting formula of Scoccimarro & Couchman (2001) with coefficients $F_2^{\rm eff}(k_1, k_2)$ described in section 2.4.3 of Takada & Jain (2004):

$$B_\delta(k_1,k_2,k_3;\chi) = 2F_2^{\rm eff}(k_1,k_2)P_\delta(k_1;\chi)P_\delta(k_2;\chi) + 2{\rm perm}. \quad (9)$$

In order to approximate the 3D intrinsic alignment bispectra, we make a direct expansion of this method, using the intrinsic alignment power spectra instead of the non-linear matter power spectrum, where

$$B_{\delta\delta\tilde{\gamma}^{\rm I}}(k_1,k_2,k_3;\chi) = 2F_2^{\rm eff}(k_1,k_2)P_{\delta\tilde{\gamma}^{\rm I}}(k_1;\chi)P_\delta(k_2;\chi) + 2F_2^{\rm eff}(k_2,k_3)P_\delta(k_2;\chi)P_{\delta\tilde{\gamma}^{\rm I}}(k_3;\chi) + 2F_2^{\rm eff}(k_3,k_1)P_{\delta\tilde{\gamma}^{\rm I}}(k_3;\chi)P_{\delta\tilde{\gamma}^{\rm I}}(k_1;\chi), \quad (10)$$

$$B_{\delta\tilde{\gamma}^{\rm I}\tilde{\gamma}^{\rm I}}(k_1,k_2,k_3;\chi) = 2F_2^{\rm eff}(k_1,k_2)P_{\tilde{\gamma}^{\rm I}}(k_1;\chi)P_{\delta\tilde{\gamma}^{\rm I}}(k_2;\chi) + 2F_2^{\rm eff}(k_2,k_3)P_{\delta\tilde{\gamma}^{\rm I}}(k_2;\chi)P_{\delta\tilde{\gamma}^{\rm I}}(k_3;\chi) + 2F_2^{\rm eff}(k_3,k_1)P_{\tilde{\gamma}^{\rm I}}(k_3;\chi)P_{\delta\tilde{\gamma}^{\rm I}}(k_1;\chi), \quad (11)$$

$$B_{\tilde{\gamma}^{\rm I}}(k_1,k_2,k_3;\chi) = 2F_2^{\rm eff}(k_1,k_2)P_{\tilde{\gamma}^{\rm I}}(k_1;\chi)P_{\tilde{\gamma}^{\rm I}}(k_2;\chi) + 2{\rm perm}. \quad (12)$$

We find that this treatment gives reasonable results for the intrinsic alignment bispectra.

We explore several methods of varying the redshift separation and orientation in the bispectrum. We can define the bispectrum triangle configuration by the redshift of its vertices ($z_1^{\rm P}$, $z_2^{\rm P}$ and $z_3^{\rm P}$) and the ℓ modes corresponding to the angular separation of its sides. From these values, we can derive the mean redshift ($\bar{z}^{\rm P}$) and the side lengths measured in redshift of each triangle ($\Delta z_1^{\rm P}$, $\Delta z_2^{\rm P}$ and $\Delta z_3^{\rm P}$), where the side $\Delta z_n^{\rm P}$ is defined opposite the vertex n with photo-z $z_n^{\rm P}$. In all cases, we keep $\bar{z}^{\rm P}$ constant. The first (Method 1) is most similar to the method employed by Zhang for the power spectrum. We set $z_2^{\rm P} = \bar{z}^{\rm P}$ constant, and instead vary $z_1^{\rm P}$ and $z_3^{\rm P}$ such that $\Delta z_1^{\rm P} = \Delta z_3^{\rm P} = \Delta z_2^{\rm P}/2$. The quantity $\Delta z_2^{\rm P}$ is then the separation that we vary, which completely defines the redshift configuration of the triangle in this method.

In Methods 2 and 3, we set $z_1^{\rm P} = z_2^{\rm P}$ such that $\Delta z_3^{\rm P} = 0$. We then vary $\Delta z_1^{\rm P} = \Delta z_2^{\rm P}$, which completely defines the triangle configuration. In the first case, Method 2, we vary the separation $\Delta z_1^{\rm P} = \Delta z_2^{\rm P}$ with $z_3^{\rm P}$ increasing in redshift. In the second case, Method 3, we instead vary the separation $\Delta z_1^{\rm P} = \Delta z_2^{\rm P}$ with $z_3^{\rm P}$ decreasing in redshift. We can also explore more complicated methods where $\Delta z_3^{\rm P}$ is constant and non-zero. We then vary $\Delta z_2^{\rm P} = |\Delta z_3^{\rm P} - \Delta z_1^{\rm P}|$. These more complicated cases do still show a large change in the intrinsic alignment bispectra with varying $\Delta z_2^{\rm P}$, but are less useful for a self-calibration of the intrinsic alignment signal as there is not a simple relationship between the intrinsic alignment and galaxy bispectra as we discuss in Section 3.

We summarize the $\Delta z^{\rm P}$ dependence of Methods 1–3 in Table 1, showing the per cent change in the magnitude of the bispectra from $\Delta z^{\rm P} = 0.0$ to 0.1 and from $\Delta z^{\rm P} = 0.0$ to 0.2. With Method 1 we find a resulting $\Delta z^{\rm P}$ dependence in the GGI and III bispectra which is similar to that found by Zhang for the GI and II power spectra, though with almost no detectable dependence in the GII bispectrum. This similarity and the reduced dependence in Method 1 when compared to Methods 2 and 3, which are described below, can be understood from the way we have varied the redshifts in this case, keeping one vertex at a fixed redshift $\bar{z}^{\rm P}$, which is very similar to the two-point case where only two points are varying in redshift. Both Methods 2 and 3 show a noticeable increase in $\Delta z^{\rm P}$ dependence, though the GGI bispectrum in Method 2 is actually less dependent than in Method 1. All three demonstrate a nearly identical per cent change over a separation of $\Delta z^{\rm P} = 0.2$ in the GGG bispectrum, at the 1–2 per cent level.

Method 3 clearly has the strongest $\Delta z^{\rm P}$ dependence. We find that this is significantly stronger than for the two-point case and both the previous methods, and so we will focus our discussion on Method 3 as the best candidate for a self-calibration of the intrinsic alignment

Table 1. The $\Delta z^{\rm P}$ dependence of $B^{\rm GGG}$ (GGG), $B^{\rm GGI} + B^{\rm GIG} + B^{\rm IGG}$ (GGI), $B^{\rm GII} + B^{\rm IGI} + B^{\rm IIG}$ (GII) and $B^{\rm III}$ (III) for the three methods of varying redshift separation described in Section 2.1. The values listed are the ratio $|B(\Delta z^{\rm P})/B(\Delta z^{\rm P} = 0)|$, showing the relative change in magnitude between $\Delta z^{\rm P} = 0.0$ and 0.1 and between $\Delta z^{\rm P} = 0.0$ and 0.2. Method 1 shows a similar $\Delta z^{\rm P}$ dependency to the power spectrum, while Method 3 clearly displays the most distinct $\Delta z^{\rm P}$ dependency.

	Method 1		Method 2		Method 3	
$\Delta z^{\rm P}$	0.1 (per cent)	0.2 (per cent)	0.1 (per cent)	0.2 (per cent)	0.1 (per cent)	0.2 (per cent)
GGG	0.5	1.5	0.5	1.5	0.5	2
GGI	12	48	12	37	20	89
GII	1	6	5	32	8	42
III	23	64	28	72	30	77

signal. As described in Table 1, we find a relative change of 8, 20 and 30 per cent in the GII, GGI and III bispectra, respectively, between $\Delta z^{\rm P} = 0.0$ and 0.1. However, this increases greatly such that between $\Delta z^{\rm P} = 0.0$ and 0.2, we find a very large relative change of 42, 77 and 89 per cent in the GII, III and GGI bispectra, respectively. The change in the GGG bispectrum is only 2 per cent between $\Delta z^{\rm P} = 0.0$ and 0.2, by comparison. This very strong $\Delta z^{\rm P}$ dependence will allow us to develop a means to self-calibration of the intrinsic alignment signal, which we describe in the following sections.

2.2 Describing the redshift separation dependence

The $\Delta z^{\rm P}$ dependence in the bispectrum as shown in equation (3) should primarily be determined by the weighting function $W^{\alpha\beta\gamma}$, which has an explicit dependence on $z_1^{\rm P}$, $z_2^{\rm P}$ and $z_3^{\rm P}$. We find this to be particularly true of the ratio $B(\Delta z^{\rm P})/B(\Delta z^{\rm P} = 0)$. This observation forms the basis for understanding the $\Delta z^{\rm P}$ dependence in $B^{\rm GGG}$ (Section 2.2.1), $B^{\rm GGI}$ (Section 2.2.4), $B^{\rm GII}$ (Section 2.2.3) and $B^{\rm III}$ (Section 2.2.2). We show in Fig. 3 the behaviour of $W^{\alpha\beta\gamma}$ as a function of true redshift for various values of $\Delta z^{\rm P}$.

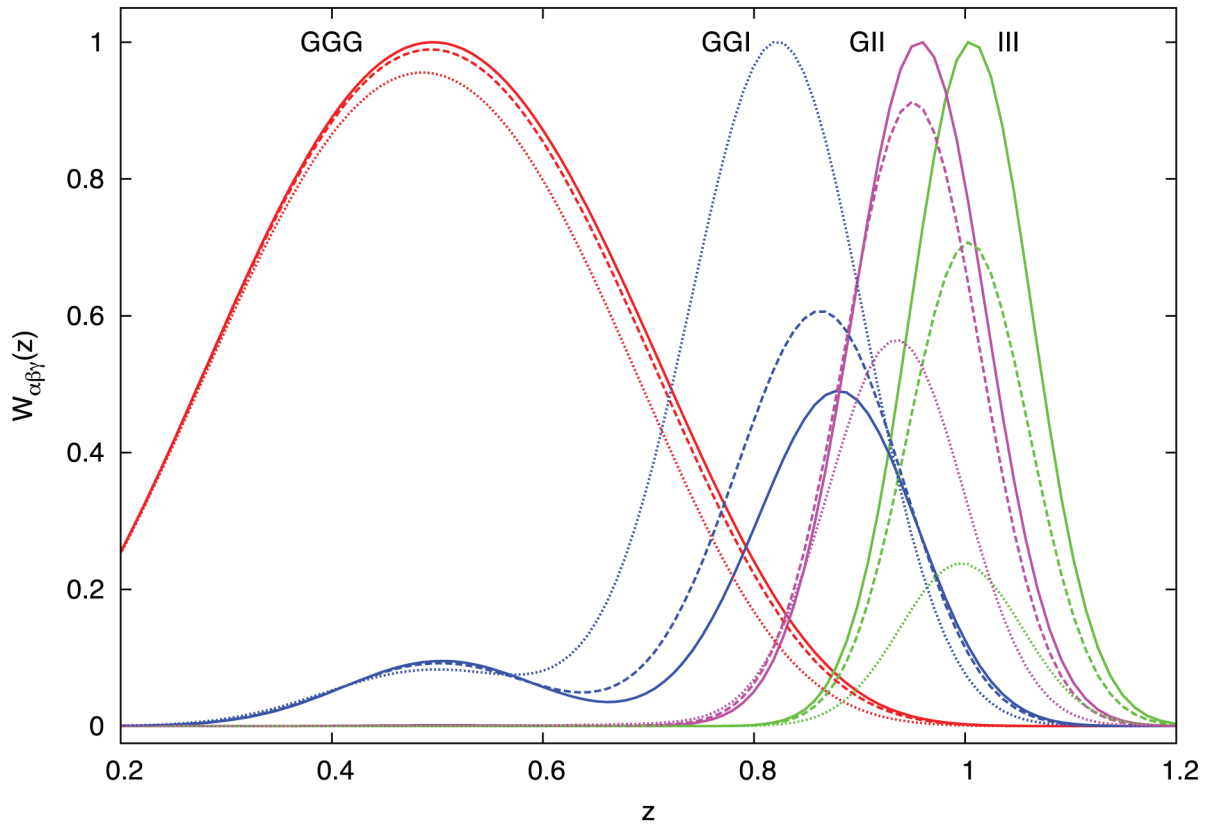

Figure 3. The weighting functions $W^{\alpha\beta\gamma}$ evaluated at $\ell = 1000$ and $\bar{z}^{\rm P} = 1.0$. The lines labelled GGG correspond to $W^{\rm GGG}$, GGI to the sum $W^{\rm GGI} + W^{\rm GIG} + W^{\rm IGG}$, GII to the sum $W^{\rm GII} + W^{\rm IGI} + W^{\rm IIG}$ and III to $W^{\rm III}$. The solid lines are evaluated with $\Delta z^{\rm P} = 0.0$, the dashed lines with $\Delta z^{\rm P} = 0.1$ and the dotted lines with $\Delta z^{\rm P} = 0.2$. There is a non-negligible contribution to the sum $W^{\rm GGI} + W^{\rm GIG} + W^{\rm IGG}$ from the fraction $p_{\rm cat}$ of outlier galaxies at $z = 0.5$.

2.2.1 *Redshift separation dependence in $B^{\rm GGG}$*

We see from Fig. 3 that $W^{\rm GGG}$, though strongly dependent on $\bar{z}^{\rm P}$, has very little dependence on $\Delta z^{\rm P}$, which explains the very small change in $B^{\rm GGG}$ as a function of $\Delta z^{\rm P}$. In the two-point case, Zhang describes the shear power spectrum with a Taylor expansion about $\Delta z^{\rm P} = 0$ up to second order, where the first derivative of the lensing spectrum with respect to $\Delta z^{\rm P}$ is shown to be zero. In the case of Method 3, it is not true that the first derivative is zero in the same way due to asymmetry. However, we can apply the same argument to our Method 1, which is symmetric, and express $B^{\rm GGG}$ as

$$\frac{B^{\rm GGG}(\Delta z^{\rm P})}{B^{\rm GGG}(\Delta z^{\rm P}=0)} \approx 1 - f_{\rm GGG}(\Delta z^{\rm P})^2,$$
$$f_{\rm GGG} \equiv \frac{\partial^2 B^{\rm GGG}(\Delta z^{\rm P})/\partial(\Delta z^{\rm P})^2|_0}{B^{\rm GGG}(\Delta z^{\rm P}=0)}. \quad (13)$$

We can apply the $f_{\rm GGG}$ calculated in this way from Method 1 to compare with the results of Method 3. We find that for $\ell = 1000$ and $\bar{z}^{\rm P} = 1$, this results in $f_{\rm GGG} = 0.67$. Using this value, we find that the approximation in equation (13) is accurate to within 1 per cent at $\Delta z^{\rm P} = 0.3$. This is demonstrated in Fig. 4, where the right-hand side of equation (13) is plotted as the dotted line labelled GGG, which nearly overlaps the left-hand side, plotted as the solid line labelled GGG. In general, we find $f_{\rm GGG} \in (0.5, 1.0)$ for $\ell \in (40, 4000)$ at $\bar{z}^{\rm P} = 1$. Alternatively, we can fit equation (13) to the calculated $B^{\rm GGG}$ and determine a best-fitting $f_{\rm GGG}$. This results in a slightly lower value of $f_{\rm GGG}$ with greatly improved accuracy, to within 0.1 per cent.

2.2.2 *Redshift separation dependence in $B^{\rm III}$*

Unlike $W^{\rm GGG}$, it is clear from Fig. 3 that $W^{\rm III}$ is strongly dependent on $\Delta z^{\rm P}$. However, the peak position in z is determined by $\bar{z}^{\rm P}$ and is insensitive to $\Delta z^{\rm P}$, as long as the photo-z is sufficiently accurate. The peak's amplitude decreases with $\Delta z^{\rm P}$, which explains the quick decrease in magnitude of $B^{\rm III}$ seen in Fig. 4 as $\Delta z^{\rm P}$ increases. This is a well-known result that is the basis for limiting measurements of the cosmic shear to only cross-correlations between thick photo-z bins in order to reduce the impact of the II, III and GII signals.

This sharp peak in $W^{\rm III}$ at $z_{\rm peak}$, which is insensitive to $\Delta z^{\rm P}$, allows us to make an approximation in the expression for $B^{\rm III}$,

$$B^{\rm III}\left(\ell; z_1^{\rm P}, z_2^{\rm P}, z_3^{\rm P}\right) = \frac{B_{\rm III}(k; \chi(z_{\rm peak}))}{\chi^4(z_{\rm peak})} \int_0^{\chi} W^{\rm III}(\chi'; \chi_1, \chi_2, \chi_3)\, {\rm d}\chi', \quad (14)$$

where the dependence on $\Delta z^{\rm P}$ is contained within the final integral. In the limit of perfect photo-z information, this $\Delta z^{\rm P}$ dependence is

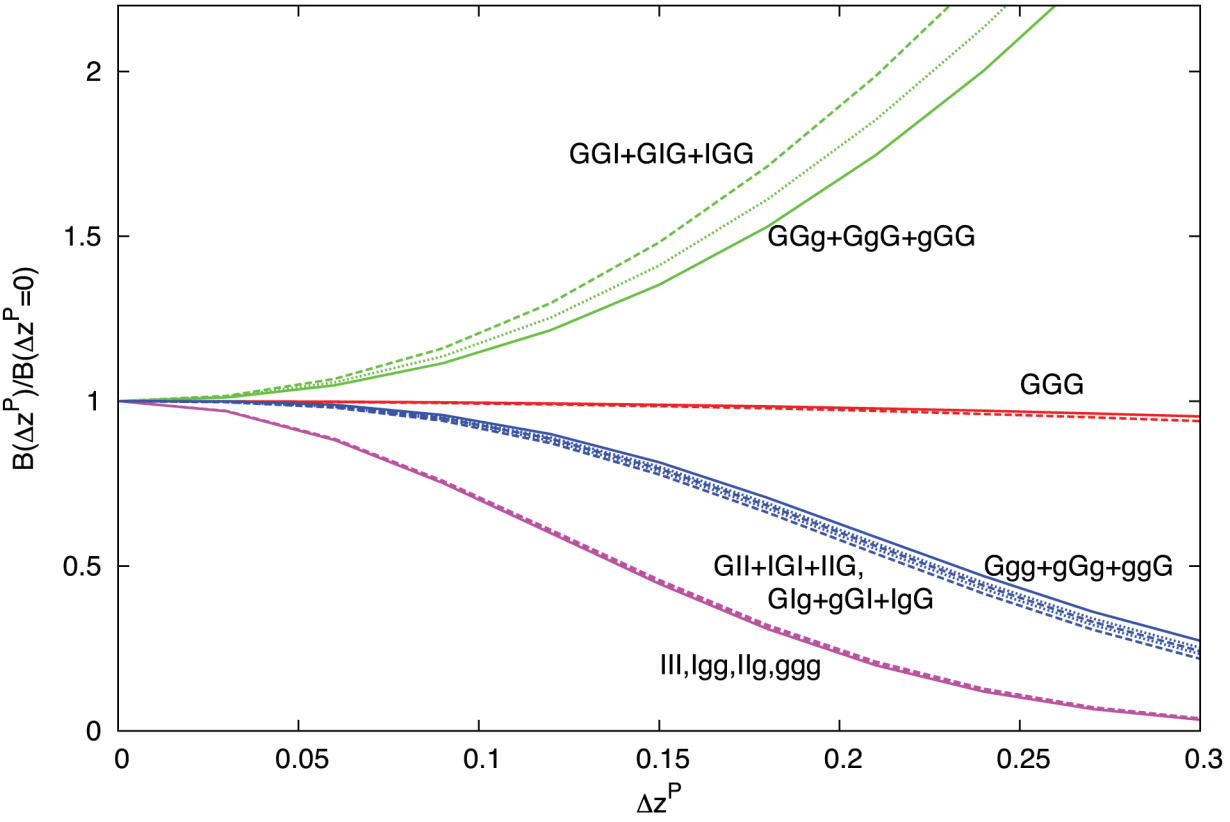

Figure 4. The ratio $B^{\alpha\beta\gamma}(\Delta z^{\rm P})/B^{\alpha\beta\gamma}(\Delta z^{\rm P} = 0)$ evaluated for the labelled $\alpha\beta\gamma$ at $\ell = 1000$ and $\bar{z}^{\rm P} = 1.0$. This demonstrates the accuracy of the relations in equations (13) and (15)–(20). The lines labelled GGG which overlap are the left-hand (solid) and right-hand (dashed) sides of equation (13). The right-hand side is evaluated as described in Section 2.2.1. The intrinsic alignment signal is evaluated using both the SB10 model and the toy model with $a = 1/2$. For GGI + GIG + IGG, GII + IGI + IIG and GIg + gGI + IgG, the dashed lines use the SB10 model while the dotted lines use the toy model. Due to the accuracy of equations (18) and (19), the lines associated with the GGI and GIg bispectra bunch very closely to the line associated with the Ggg bispectrum. Similarly, the lines labelled III, IIg, Igg and ggg overlap due to the high accuracy of equations (15)–(17). The relatively strong $\Delta z^{\rm P}$ dependencies of the various bispectra compared to that of GGG can be understood by comparing the effects of different $\Delta z^{\rm P}$ on the weighting functions in Fig. 3, which cause a strong decrease (or increase) in the amplitudes of $W^{\rm GGI}$, $W^{\rm GII}$ and $W^{\rm III}$. The relative differences in the lines associated with the GGI (GGg) and GII (Ggg) bispectra are contributed to by both the different redshift dependencies of the two intrinsic alignment models, as well as the stronger dependence of the peak positions of $W^{\rm GGI}$ and $W^{\rm GII}$ on redshift separation in Fig. 3, which decreases the accuracy of the approximation in equations (20) and (18).

exact. It is now clear that since $W^{\rm III} = W^{\rm ggg}$, we can relate $B^{\rm III}$ and $B^{\rm ggg}$ as

$$B^{\rm III}\left(\ell; z_1^{\rm P}, z_2^{\rm P}, z_3^{\rm P}\right) = A_{\rm III}\left(\ell; z_1^{\rm P}, z_2^{\rm P}, z_3^{\rm P}\right) B^{\rm ggg}\left(\ell; z_1^{\rm P}, z_2^{\rm P}, z_3^{\rm P}\right), \quad (15)$$

where $A_{\rm III} \equiv B_{\rm III}(k; \chi(z_{\rm peak}))/B_{\rm ggg}(k; \chi(z_{\rm peak}))$. We propose to work with this relationship because it is in practice more accurate than equation (14), and because the same lensing survey will measure $B^{\rm ggg}$ in addition to the shear bispectrum. This tells us directly the $\Delta z^{\rm P}$ dependence in $B^{\rm III}$ without any knowledge of the photo-z PDF or intrinsic alignment being necessary. In the same way, we can construct the following relationships as well:

$$B^{\rm IIg}\left(\ell; z_1^{\rm P}, z_2^{\rm P}, z_3^{\rm P}\right) = A_{\rm IIg}\left(\ell; z_1^{\rm P}, z_2^{\rm P}, z_3^{\rm P}\right) B^{\rm ggg}\left(\ell; z_1^{\rm P}, z_2^{\rm P}, z_3^{\rm P}\right), \quad (16)$$

$$B^{\rm Igg}\left(\ell; z_1^{\rm P}, z_2^{\rm P}, z_3^{\rm P}\right) = A_{\rm Igg}\left(\ell; z_1^{\rm P}, z_2^{\rm P}, z_3^{\rm P}\right) B^{\rm ggg}\left(\ell; z_1^{\rm P}, z_2^{\rm P}, z_3^{\rm P}\right). \quad (17)$$

Fig. 4 compares the $\Delta z^{\rm P}$ dependence of $B^{\rm III}$, $B^{\rm IIg}$, $B^{\rm Igg}$ and $B^{\rm ggg}$ and shows that equations (15)–(17) are accurate to within 1 per cent at $\Delta z^{\rm P} = 0.2$. As with $f_{\rm GGG}$, we will treat $A_{\rm III}$, $A_{\rm IIg}$ and $A_{\rm Igg}$ as free parameters in order to avoid modelling uncertainty in the self-calibration discussed in Section 3.

2.2.3 Redshift separation dependence in $B^{\rm GII}$

We find that the sum $W^{\rm GII} + W^{\rm IGI} + W^{\rm IIG}$ behaves very similarly to $W^{\rm III}$, as shown in Fig. 3, except for a slightly greater dependence in peak position due to $\Delta z^{\rm P}$ and much less dependence on $\Delta z^{\rm P}$ in peak amplitude. We thus propose a similar relationship to that described in equation (15) for $B^{\rm III}$, which is further motivated by the $\Delta z^{\rm P}$ dependence of $B^{\rm GII} + B^{\rm IGI} + B^{\rm IIG}$ in Fig. 4, when compared to $B^{\rm Ggg} + B^{\rm gGg} + B^{\rm ggG}$. Leaving out explicit dependence on ℓ and $z_1^{\rm P}$, $z_2^{\rm P}$, $z_3^{\rm P}$, this relationship is approximately

$$B^{\rm GII} + B^{\rm IGI} + B^{\rm IIG} \approx A_{\rm GII}\left[B^{\rm Ggg} + B^{\rm gGg} + B^{\rm ggG}\right]. \quad (18)$$

In the same way, we can construct

$$B^{\rm GIg} + B^{\rm gGI} + B^{\rm IgG} \approx A_{\rm GIg}\left[B^{\rm Ggg} + B^{\rm gGg} + B^{\rm ggG}\right]. \quad (19)$$

Due to the peak being less sharp as compared to that for $B^{\rm III}$ and there being a stronger dependence on $\Delta z^{\rm P}$ in the peak position, these relationships are not as exact as equations (15)–(17). We still find a large degree of accuracy, however, with equation (18) being accurate to within 5 per cent and equation (19) being accurate to within 3 per cent at $\Delta z^{\rm P} = 0.2$.

2.2.4 Redshift separation dependence in $B^{\rm GGI}$

Unlike $W^{\rm III}$ and $W^{\rm GII} + W^{\rm IGI} + W^{\rm IIG}$, the peak of the sum $W^{\rm GGI} + W^{\rm GIG} + W^{\rm IGG}$ does clearly depend on $\Delta z^{\rm P}$ as shown in Fig. 3, though with a greater dependence in peak amplitude on $\Delta z^{\rm P}$ compared to the sum $W^{\rm GII} + W^{\rm IGI} + W^{\rm IIG}$ and $W^{\rm III}$, instead increasing in amplitude with decreasing $\Delta z^{\rm P}$. There is also a non-negligible contribution from the fraction $p_{\rm cat}$ of outlier galaxies in equation (7) around $z = 0.5$. However, from Fig. 4, we still find a similar dependence on $\Delta z^{\rm P}$ between $B^{\rm GGI} + B^{\rm GIG} + B^{\rm IGG}$ and $B^{\rm GGg} + B^{\rm GgG} + B^{\rm gGG}$, so we propose the relationship

$$B^{\rm GGI} + B^{\rm GIG} + B^{\rm IGG} \approx A_{\rm GGI}\left[B^{\rm GGg} + B^{\rm GgG} + B^{\rm gGG}\right]. \quad (20)$$

While this relationship is much less accurate than equations (15)–(18), due to the assumption that $z_{\rm peak}$ is constant being less valid for GGI, it still is accurate to within 5 per cent at $\Delta z^{\rm P} = 0.1$ and 20 per cent at $\Delta z^{\rm P} = 0.2$. Thus, if we wish to work at the accuracy possible for the two-point case as shown by Zhang (2010b), where at $\Delta z^{\rm P} = 0.2$ the largest inaccuracy is about 10 per cent in the GI term, we must limit ourselves to $\Delta z^{\rm P} \approx 0.13$. Alternatively, we can use the limit proposed by Zhang of $\Delta z^{\rm P} \approx 0.2$, but with a loss of accuracy in equation (20) of a factor of 2 when compared to the two-point GI–Gg relationship.

We can see from Fig. 4 that the accuracy of equation (20) could be improved by making assumptions about the redshift dependency of the intrinsic alignment or by measuring it independently. We could also include in the coefficient $A_{\rm GGI}$ an extra dependency on redshift, instead of the simple scaling relationship we have assumed, which could account for redshift-dependent sources of error like the changing position of $z_{\rm peak}$ for GGI. This would introduce more free parameters into the self-calibration but would also allow the use of larger $\Delta z^{\rm P}$. The choice of whether to include either intrinsic alignment model assumptions, additional measurements of redshift dependencies in the intrinsic alignment, additional free parameters in the self-calibration, or some combination of these or other assumptions will impact both the choice of upper $\Delta z^{\rm P}$ and the ultimate performance of the self-calibration, but this choice must be made with the requirements of a particular lensing survey in mind. For this reason, we will limit our discussion to the basic framework developed in this section when addressing the performance of the self-calibration in Section 3.1.

3 INTRINSIC ALIGNMENT SELF-CALIBRATION

We can now consider a means to self-calibrate the intrinsic alignment signal, by using the four measurable bispectra between galaxy ellipticity and galaxy density in a weak lensing survey, with negligible magnification bias, as discussed in Troxel & Ishak (2012a):

$$B^{(1)} = B^{\rm GGG} + B^{\rm GGI} + 2{\rm perm.} + B^{\rm GII} + 2{\rm perm.} + B^{\rm III}, \quad (21)$$

$$B^{(2)} = B^{\rm GGg} + 2{\rm perm.} + B^{\rm GIg} + 2{\rm perm.} + B^{\rm IIg}, \quad (22)$$

$$B^{(3)} = B^{\rm Ggg} + 2{\rm perm.} + B^{\rm Igg}, \quad (23)$$

$$B^{(4)} = B^{\rm ggg}. \quad (24)$$

Equation (21) is the measured galaxy ellipticity–ellipticity–ellipticity bispectrum, which measures both cosmic shear and correlated intrinsic alignment. In the case of no intrinsic alignment contamination, $B^{(1)}$ is simply the shear bispectrum, $B^{\rm GGG}$, and should be effectively independent of $\Delta z^{\rm P}$ within measurement error. However, we expect $B^{(1)}$ to have a measurable dependence on $\Delta z^{\rm P}$ at minimum survey error with even just a few per cent or more contamination by intrinsic alignment due to the very strong $\Delta z^{\rm P}$ dependence of the intrinsic alignment bispectra. We explore this in Fig. 5, where we plot both $B^{\rm GGG}$ and $B^{(1)}$ for 1, 5, 10 and 20 per cent levels of intrinsic alignment contamination for both the SB10 model and the toy model. We are interested in the total absolute impact of the intrinsic alignment as a fraction of $B^{(1)}$, since this (and not the individual intrinsic alignment components) is what impacts cosmological information, and so we measure the contamination as $|B^{(1)} - B^{\rm GGG}|/B^{(1)}$. Error bars representing the expected minimum measurement uncertainty in an LSST-like survey are shown on $B^{\rm GGG}$. The measurement uncertainty in $B^{\rm GGG}$ is extrapolated from the expected error found by Zhang (2010b) for the power spectrum

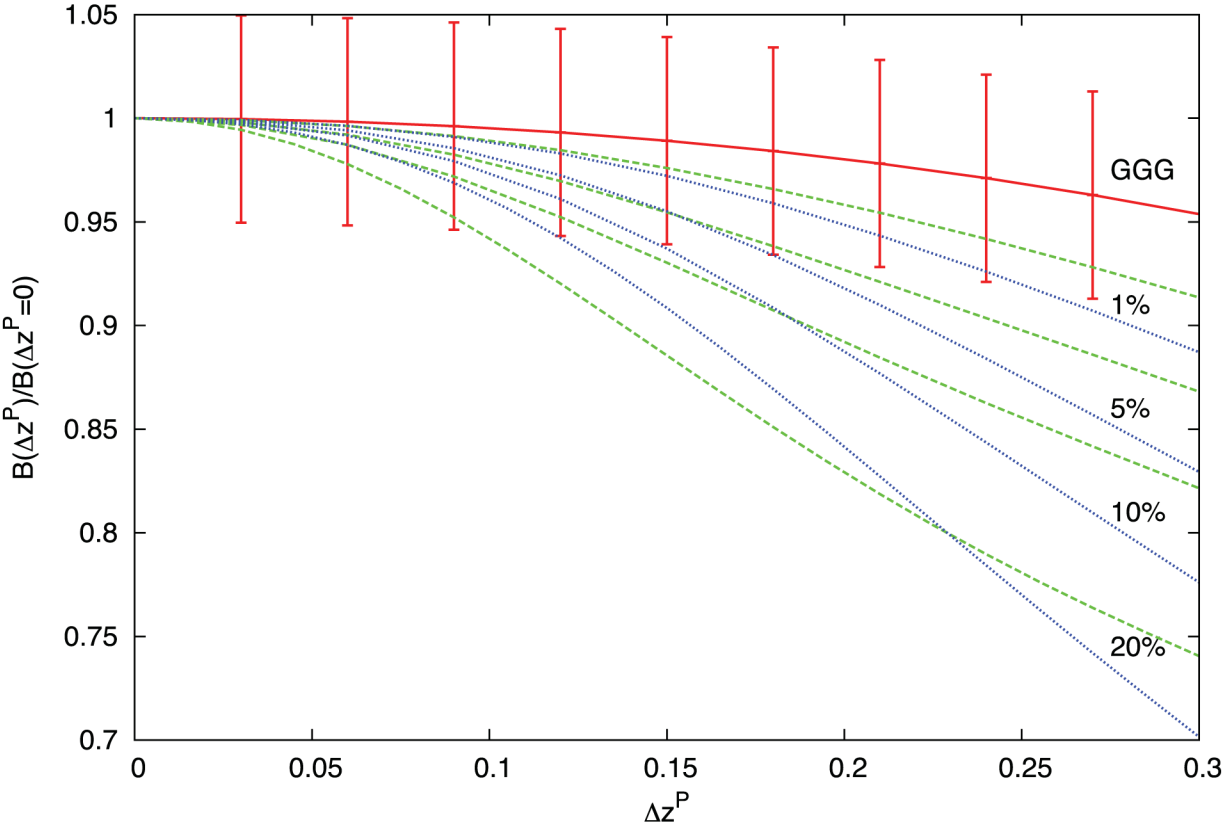

Figure 5. The ratio $B^{(1)}(\Delta z^{\rm P})/B^{(1)}(\Delta z^{\rm P}=0)$, where $B^{(1)}=B^{\rm GGG}+B^{\rm GGI}+B^{\rm GII}+B^{\rm III}$, and the intrinsic alignment signal is modelled with both the SB10 model (dashed) and the toy model with $a=1/2$ (dotted) for $\ell=1000$ and $\bar{z}^{\rm P}=1.0$. From top to bottom, levels of total intrinsic alignment contamination $|B^{(1)}-B^{\rm GGG}|/B^{(1)}$ of 1, 5, 10 and 20 per cent are shown. We are interested in the total absolute impact of the intrinsic alignment as a fraction of $B^{(1)}$, since this (and not the individual intrinsic alignment components) is what impacts cosmological information. For comparison, we show $B^{\rm GGG}$ (solid) with the expected minimum measurement uncertainty for an LSST-like survey. At this level of uncertainty, we find that it is possible to identify the presence of even a small intrinsic alignment contamination of a few per cent at $\Delta z^{\rm P}=0.2$.

of LSST, modifying the derivation of Troxel & Ishak (2012a) for the lensing bispectrum in a single redshift bin.

Given simultaneous measurements of equations (21)–(24) in small redshift bins of size ∼0.01 at seven or more $\Delta z^{\rm P}$, along with the relations in equations (13) and (15)–(20), we can now simultaneously reconstruct $B^{\rm GGG}$, $B^{\rm GGI}$, $B^{\rm GII}$ and $B^{\rm III}$ through the observables given in equations (21)–(24) and with free parameters $f_{\rm GGG}$, $A_{\rm GGI}$, $A_{\rm GII}$, $A_{\rm GIg}$, $A_{\rm III}$, $A_{\rm Igg}$ and $A_{\rm IIg}$. In practice, it is more useful to measure the total contamination $B^{\rm GGI}+B^{\rm GII}+B^{\rm III}$, which can be determined to higher accuracy due to a partial degeneracy between the three intrinsic alignment bispectra. As we show in Fig. 4, this is because all three cause $B^{(1)}$ to decrease with $\Delta z^{\rm P}$. $B^{\rm III}$ and $B^{\rm GII}$ + perm. clearly decrease with $\Delta z^{\rm P}$, and though $B^{\rm GGI}$ + perm. increases with $\Delta z^{\rm P}$, its magnitude is negative, and so it also causes $B^{(1)}$ to decrease with $\Delta z^{\rm P}$. Though we have concentrated on a particular ℓ and $\bar{z}^{\rm P}$, $\Delta z^{\rm P}$ has a weak dependence on scale and mean redshift, so that we expect the self-calibration to be generally applicable to a wide range of values.

3.1 Performance of the self-calibration

From Fig. 3, we see that to good approximation $B^{\alpha\beta\gamma}$ samples the same cosmic volume for different $\Delta z^{\rm P}$, which means that different $\Delta z^{\rm P}$ should share the same cosmic variance as found for the power spectrum (Zhang 2010b). Relative differences due to cosmic variance are thus $<\sqrt{2\pi^2}(\ell^3\Delta\ell^3 f_{\rm sky})^{-1/2}=1.4\times10^{-5}$ per cent $(10^3/\ell)^{3/2}(10^2/\Delta\ell)^{3/2}f_{\rm sky}^{-1/2}$, and so are negligible compared to the >5 per cent change in $B^{(1)}$ over $\Delta z^{\rm P}=0.2$ for intrinsic alignment contaminations of >1 per cent. However, the shot noise due to random galaxy shapes is large compared to the cosmic variance at large ℓ, for small redshift bins ∼0.01 with a typical number of galaxies 2.5×10^7 at $\bar{z}^{\rm P}=1.0$ for LSST (Zhan, Knox & Tyson 2009). It must be controlled in order to reach the necessary precision in order to identify the $\Delta z^{\rm P}$ dependence at low levels of intrinsic alignment contamination. This is complicated by the fact that unlike cosmic variance, shot noise is uncorrelated at different $\Delta z^{\rm P}$. Zhang (2010b) discusses a means to reduce the shot noise by averaging over larger ℓ bins at varying $\bar{z}^{\rm P}$, since the $\Delta z^{\rm P}$ dependence is weak across ℓ and $\bar{z}^{\rm P}$ for the power spectrum. We find this to be accurate for the bispectrum as well, and expect this method to be applicable in the three-point self-calibration in order to reduce the shot noise to manageable levels in the small photo-z bins necessary for the self-calibration. We also anticipate the self-calibration to be applicable in the presence of other errors which have different $\Delta z^{\rm P}$ dependencies.

In order for the self-calibration to reconstruct the intrinsic alignment signal in this way, with some associated error which is due primarily to the inaccuracy in equations (20) and (18), we must be able to measure seven or more $\Delta z^{\rm P}$ in ∼0.01 photo-z bins which are distinct from the measurement error. If we consider the expected measurement error for LSST shown in Fig. 5, we would be able to achieve the necessary measurements to self-calibrate the

intrinsic alignment signal for intrinsic alignment contaminations of ∼10 per cent or more for maximum $\Delta z^{\rm P} = 0.2$. If we instead accept a greater inaccuracy in equations (20) and (18) at higher $\Delta z^{\rm P}$, it would then be possible to measure smaller intrinsic alignment contaminations. The precise choice between maximum $\Delta z^{\rm P}$ and error in the final intrinsic alignment measurement through the self-calibration will then be entirely dependent upon the specific capabilities of the survey as well as the goals of the measurement. For example, if the resulting intrinsic alignment bispectrum is intended to constrain models of structure formation or intrinsic alignment models, then a lower maximum $\Delta z^{\rm P}$ might be imposed in order to achieve better accuracy in the intrinsic alignment measurement.

3.2 Other sources of uncertainty

The results of the previous section are dependent upon the accuracy of our assumptions in the quantitative calculations regarding the performance of the self-calibration. For the bispectrum, we have used an approximate fitting formula derived from perturbation theory by Scoccimarro & Couchman (2001) in our performance estimations, and we have chosen a specific set of intrinsic alignment models. We also use a deterministic approach to modelling the galaxy bias, which is not perfectly accurate in real galaxy distributions. Failures in either these assumptions or the accuracy of the models for the intrinsic alignment bispectra would lead to additional uncertainty in the expected performance of the self-calibration, which may impact its applicability depending on the degree to which the assumptions or models fail. However, Baldauf et al. (2010) have shown that it is possible to suppress the galaxy stochasticity to the 1 per cent level in some cases, which would be safely negligible compared to other sources of error we have discussed above. We have also chosen two very different models of the intrinsic alignment, in order to minimize bias in the resulting performance evaluation.

4 CONCLUSION

The strong $\Delta z^{\rm P}$ dependency of the intrinsic alignment signal for large bin size $\geq$0.2 has been used to motivate the preference of cross-spectra and bispectra between redshift bins in order to reduce the intrinsic alignment contamination. This has previously been used as a means to neglect the III and GII bispectra and II spectrum in techniques developed to remove the intrinsic alignment contamination from the lensing signal using information between redshift bins (Joachimi & Schneider 2008, 2009, 2010; Shi et al. 2010; Zhang 2010a; Troxel & Ishak 2012a). In this work, we instead use this $\Delta z^{\rm P}$ dependency within a single redshift bin of size $\geq$0.2 to self-calibrate the measured galaxy ellipticity–ellipticity–ellipticity bispectrum, reconstructing simultaneously not only the cosmic shear bispectrum (GGG), but also the intrinsic alignment GGI, GII and III bispectra.

We first explore several means of defining and measuring the $\Delta z^{\rm P}$ dependence in the lensing and intrinsic alignment bispectra $B^{\rm GGG}$, $B^{\rm GGI}$, $B^{\rm GII}$ and $B^{\rm III}$, and show in Fig. 4 the resulting $\Delta z^{\rm P}$ dependency of the best method as well as the accuracy of the scaling relations in equations (15)–(20). These relate the intrinsic alignment to the directly measurable galaxy density through a set of simple scaling parameters. This is true for both the toy model and the SB10 model of intrinsic alignment clustering, which have very different dependencies on both scale and redshift. We further show that unlike the intrinsic alignment bispectra, $B^{\rm GGG}$ is effectively independent of $\Delta z^{\rm P}$, which means a measured $\Delta z^{\rm P}$ dependence in the measured ellipticity bispectrum is a clear indication of the presence of intrinsic alignment.

Using the measured cross-correlation galaxy ellipticity and galaxy density bispectra in a weak lensing survey, as well as the scaling relations in equations (15)–(20), we propose a simple self-calibration method to simultaneously reconstruct the GGG, GGI, GII and III bispectra. The proposed self-calibration method relies only on the information already gathered by a weak lensing survey and makes no assumptions on the modelling of intrinsic alignment or photo-z PDF, instead depending on the relationship between the intrinsic alignment and galaxy density signals. We explore the feasibility and proposed structure of the self-calibration, including limitations on maximum $\Delta z^{\rm P}$ due to the inaccuracy of equations (20) and (18), and discuss some means of addressing it. We find that $\Delta z^{\rm P} \leq 0.2$ is sufficient for accuracy in equation (20) better than 20 per cent. The precision of survey measurements of the lensing bispectrum also limits the applicability of the self-calibration, but we find that for the expected measurement error in LSST, we can reconstruct the intrinsic alignment signal for contaminations of 10 per cent at $\Delta z^{\rm P} = 0.2$, or for even smaller intrinsic alignment contaminations, but with less accuracy in the reconstructed intrinsic alignment signal. Thus, this would allow the self-calibration technique to significantly reduce the contamination of the intrinsic alignment to the weak lensing spectrum and bispectrum. However, further work is still necessary to precisely evaluate the quantitative performance of the self-calibration method in a realistic survey and its anticipated reduction in the effects of the intrinsic alignment contamination on cosmological study.

The proposed self-calibration is complimentary to existing proposals for estimating the intrinsic alignment contamination to the bispectrum, which instead depend on information between redshift bins. It can be combined with these other methods which make use of redshift tomography to better constrain the intrinsic alignment contamination without overusing the information contained within the survey. By allowing the full reconstruction of the GII and III bispectra in addition to the GGG and GGI bispectra, while not relying on assumptions of an intrinsic alignment model, it also presents a means of indirectly measuring the intrinsic alignment signal, which will be applicable to constraining proposed intrinsic alignment models and our understanding of structure formation.

ACKNOWLEDGMENTS

We thank P. Zhang for suggesting this project, L. King for useful comments and A. Peel for proofreading this paper. MI acknowledges that this material is based upon work supported in part by National Science Foundation under grant AST-1109667 and NASA under grant NNX09AJ55G, and that part of the calculations for this work have been performed on the Cosmology Computer Cluster funded by the Hoblitzelle Foundation.

REFERENCES

Acquaviva V., Hajian A., Spergel D., Das S., 2008, Phys. Rev. D, 78, 043514
Bacon D. J., Refregier A. R., Ellis R. S., 2000, MNRAS, 318, 625
Bacon D. J., Refregier A., Clowe D., Ellis R. S., 2001, MNRAS, 325, 1065
Baldauf T., Smith R., Seljak U., Mandelbaum R., 2010, Phys. Rev. D, 81, 063531
Bean R., Tangmatitham M., 2010, Phys. Rev. D, 81, 083534
Bernstein G. M., Huterer D., 2009, MNRAS, 401, 1399
Bernstein G. M., Jarvis M., 2002, AJ, 123, 583
Blazek J., McQuinn M., Seljak U., 2011, J. Cosmol. Astropart. Phys., 05, 010

Bridle S., King L., 2007, New J. Phys., 9, 444
Brown M. L., Taylor A. N., Hambly N. C., Dye S., 2002, MNRAS, 333, 501
Brown M. L., Taylor A. N., Bacon D. J., Gray M. E., Dye S., Meisenheimer K., Wolf C., 2003, MNRAS, 341, 100
Capozziello S., Cardone V. F., Troisi A., 2006, Phys. Rev. D, 73, 104019
Catelan P., Kamionkowski M., Blandford R. D., 2001, MNRAS, 320, L7
Crittenden R. G., Natarajan P., Pen U.-L., Theuns T., 2001, ApJ, 559, 552
Croft R., Metzler C., 2000, ApJ, 545, 561
Daniel S., Caldwell R., Cooray A., Melchiorri A., 2008, Phys. Rev. D, 77, 103513
Daniel S., Linder E., Smith T., Caldwell R., Corray A., Leauthaud A., Lombriser L., 2010, Phys. Rev. D, 80, 123508
Dossett J., Moldenhauer J., Ishak M., 2011, Phys. Rev. D, 84, 023012
Eisenstein D. J., Hu W., Tegmark M., 1999, ApJ, 518, 2
Erben T., Van Waerbeke L., Bertin E., Mellier Y., Schneider P., 2001, A&A, 366, 717
Faltenbacher A., Li C., White S. D. M., Jing Y. P., Mao S., Wang J., 2009, Res. Astron. Astrophys., 9, 41
Fu X., Wu P., Yu H., 2009, Phys. Lett. B, 677, 12
Hearin A. P., Zentner A. R., Ma Z., Huterer D., 2010, ApJ, 720, 1351
Heavens A., Refregier A., Heymans C., 2000, MNRAS, 319, 649
Heymans C., Heavens A., 2003, MNRAS, 339, 711
Heymans C., Brown M., Heavens A., Meisenheimer K., Taylor A., Wolf C., 2004, MNRAS, 347, 895
Heymans C., White M., Heavens A., Vale C., Van Waerbeke L., 2006, MNRAS, 371, 750
Hirata C. M., Seljak U., 2003a, MNRAS, 343, 459
Hirata C. M., Seljak U., 2003b, Phys. Rev. D, 67, 43001
Hirata C. M., Seljak U., 2004, Phys. Rev. D, 70, 063526
Hirata C. M., Mandelbaum R., Ishak M., Seljak U., Nichol R., Pimbblet K. A., Ross N. P., Wake D., 2007, MNRAS, 381, 1197
Hoekstra H., Yee H. K. C., Gladders M. D., Barrientos L. F., Hall P. B., Infante L., 2002, ApJ, 72, 55
Hu W., 2002, Phys. Rev. D, 65, 023003
Hu W., Tegmark M., 1999, ApJ, 514, L65
Huterer D., Linder E., 2007, Phys. Rev. D, 75, 023519
Huterer D., Komatsu E., Shandera S., 2010, Advances Astron., 2010, 697147
Ishak M., 2005, MNRAS, 363, 469
Ishak M., 2007, Foundation Phys. J., 37, 1470
Ishak M., Dossett J., 2009, Phys. Rev. D, 80, 043004
Ishak M., Hirata C. M., McDonald P., Seljak U., 2004, Phys. Rev. D, 69, 083514
Ishak M., Upadhye A., Spergel D., 2006, Phys. Rev. D, 74, 043513
Jarvis M., Bernstein G. M., Fischer P., Smith D., Jain B., Tyson J. A., Wittman D., 2003, AJ, 125, 1014
Jeong D., Komatsu E., 2009, ApJ, 703, 1230
Jing Y. P., 2002, MNRAS, 335, 89
Joachimi B., Bridle S., 2010, A&A, 523, A1
Joachimi B., Schneider P., 2008, A&A, 488, 829
Joachimi B., Schneider P., 2009, A&A, 507, 105
Joachimi B., Schneider P., 2010, A&A, 517, A4
Joachimi B., Mandelbaum R., Abdalla F., Bridle S., 2010, A&A, 527, A26
Joudaki S., Cooray A., Holz D. E., 2009, Phys. Rev. D, 80, 023003
King L., 2005, A&A, 441, 47
King L., Schneider P., 2002, A&A, 396, 411
King L., Schneider P., 2003, A&A, 398, 23
Kirk D., Bridle S., Schneider M., 2010, MNRAS, 408, 1502
Krause E., Hirata C. M., 2011, MNRAS, 410, 2730
Linder E., Cahn R., 2007, Astropart. Phys., 28, 481
Ma Z., Bernstein G., 2008, ApJ, 682, 39
Mandelbaum R., Hirata C. M., Ishak M., Seljak U., Brinkmann J., 2006, MNRAS, 367, 611
Massey R., Refregier A., Bacon D., Ellis R., 2005, MNRAS, 359, 1277
Matarrese S., Verde L., Jimenez R., 2000, ApJ, 541, 10
Munshi D., van Waerbeke L., Smidt J., Coles P., 2012, MNRAS, 419, 536
Okumura T., Jing Y. P., 2009, ApJ, 694, L83
Pen U.-L., Lu T., Van Waerbeke L., Mellier Y., 2003, MNRAS, 346, 994
Refregier A., 2003, ARA&A, 41, 645
Rhodes J., Refregier A., Groth E. J., 2001, ApJ, 552, L85
Schmidt F., 2008, Phys. Rev. D, 78, 043002
Schneider M. D., Bridle S., 2010, MNRAS, 402, 2127 (SB10)
Schrabback T. et al., 2010, A&A, 516, A63
Scoccimarro R., Couchman H., 2001, MNRAS, 325, 1312
Semboloni E., Heymans C., van Waerbeke L., Schneider P., 2008, MNRAS, 388, 991
Semboloni E., Schrabback T., van Waerbeke L., Vafaei S., Hartlap J., Hilbert S., 2010, MNRAS, 410, 143
Shi X., Joachimi B., Schneider P., 2010, A&A, 523, A60
Song Y. S., 2005, Phys. Rev. D, 71, 024026
Takada M., Jain B., 2003, MNRAS, 340, 580
Takada M., Jain B., 2004, MNRAS, 348, 897
Takada M., White M., 2004, ApJ, 601, L1
Tereno I., Semboloni E., Schrabback T., 2010, A&A, 530, A68
Thomas S., Abdalla F., Weller J., 2009, MNRAS, 395, 197
Troxel M. A., Ishak M., 2012a, MNRAS, 419, 1804
Troxel M. A., Ishak M., 2012b, MNRAS, submitted
Upadhye A., Ishak M., Steinhardt P. J., 2005, Phys. Rev. D, 72, 063501
Vafaei S., Lu T., van Waerbeke L., Semboloni E., Heymans C., Pen U.-L., 2010, Astropart. Phys., 32, 340
Van Waerbeke L., Mellier Y., 2003, preprint (astro-ph/0305089)
Van Waerbeke L. et al., 2000, A&A, 358, 30
Van Waerbeke L., Mellier Y., Pell R., Pen U.-L., McCracken H. J., Jain B., 2002, A&A, 393, 369
Verde L., Jimenez R., Kamionkowski M., Matarrese S., 2001, MNRAS, 325, 412
Zaldarriaga M., Spergel D. N., Seljak U., 1997, ApJ, 488, 1
Zhan H., Knox L., Tyson J. A., 2009, ApJ, 690, 923
Zhang P., 2010a, ApJ, 720, 1090
Zhang P., 2010b, MNRAS, 406, L95
Zhang P. J., Liguori M., Bean R., Dodelson S., 2007, Phys. Rev. Lett., 99, 141302
Zhao H., Bacon D. J., Taylor A. N., Horne K., 2006, MNRAS, 368, 171
Zhao G., Pogosian L., Silvestri A., Zylberberg J., 2009, Phys. Rev. D, 79, 083513

This paper has been typeset from a TEX/LATEX file prepared by the author.